Multi-Beam Design for Extremely Large-Scale RIS Aided Near-Field Wireless Communications

Decai Shen and Linglong Dai

Beijing National Research Center for Information Science and Technology (BNRist)
Department of Electronic Engineering, Tsinghua University, Beijing 100084, China
Email: sdc18@mails.tsinghua.edu.cn, daill@tsinghua.edu.cn

GLOBECOM 2022 - 2022 IEEE Global Communications Conference | 978-1-6654-3540-6/22/$31.00 ©2022 IEEE | DOI: 10.1109/GLOBECOM48099.2022.10000922

***Abstract*—The development of reconfigurable intelligent surface (RIS) will evolve towards the extremely large-scale RIS (XL-RIS) to overcome the "multiplicative fading effect". With the increase in array aperture, this evolution leads to the near-field propagation becoming dominant. To achieve the performance gain of XL-RIS, it is effective to explore the near-field beam design with a codebook via beam training. Unfortunately, due to the constant modulus constraint of XL-RIS, most of the existing works in the near-field scenario focus on single-beam design. Hence, these works will face a serious loss for the quality of service in the multiple user equipments case. In this paper, we propose a block coordinate descent (BCD) based scheme with majorization-minimization (MM) algorithm for the multi-beam design. The proposed scheme handles the constant modulus constraint from two aspects. Firstly, the multi-beam design is an intractable non-convex quadratic programming problem due to this constraint. We utilize the MM algorithm to decompose this problem as a series of tractable sub-problems to be iteratively solved. Secondly, the solution space for the multi-beam design is limited due to this constraint, we introduce the phases for beam gains as an extra optimizable variable to enrich the degree of freedom for optimization. Simulation results show that the proposed multi-beam design can achieve a superior quality of service 50% higher than the existing schemes.**

I. Introduction

Reconfigurable intelligent surface (RIS) has been emerging with extensive potential to create a controllable reflecting link [1], [2]. However, the performance gain of practical RIS-aided wireless communications will be heavily restricted due to the "multiplicative fading effect" [3]. This is because the serious path loss of the reflecting link is the *multiplication* (rather than the *sum*) of the path losses of the transmitter-RIS link and the RIS-receiver link. Considering that the array gain for RIS is proportion to the square of the number of RIS elements [3], we can compensate for the path loss by enlarging the array aperture with a massive number of RIS elements. As a consequence, the evolution of RIS will perhaps develop towards extremely large-scale RIS (XL-RIS) for the future 6G wireless communications [4].

This evolution will lead to not only the enlargement of array aperture but also the critical change in the electromagnetic propagation feature from far-field to near-field [4]. To exploit the potential gain of XL-RIS, it is crucial to elaborately design the near-field XL-RIS beamforming schemes. Relying on the accurate channel state information (CSI), the XL-RIS beamforming can be formulated as a series of optimization problems like [5]. However, the accurate acquisition for CSI of the near-field channel is pretty difficult due to the computational complexity [6].

As another kind of scheme, it is effective to directly determine the near-field beam design with a codebook via beam training [6], [7]. In [6], a single-beam design codebook for the XL-RIS is discussed and a hierarchical training scheme is proposed. Moreover, in [7], a variable-width hierarchical codebook is devised which is suitable for both the near- and far-field. However, the above schemes are proposed for single-beam design and are difficult to be migrated to serve multiple user equipments (UEs). This is mainly because most of the practical XL-RIS (or RIS) can only adjust the phase coefficient rather than the amplitude coefficient [4], as called the constant modulus constraint. Due to this constraint, the solution space of the beamforming vector for multi-beam design cannot be projected onto the linear space. If we directly design the multiple beams according to the existing schemes [6], [7], the effective directions of the multiple beams will seriously deviate from the desired directions of UEs. As a consequence, the quality of service (e.g., the minimal rate of all UEs) will be rapidly decreased limited by the beam deviation, resulting in a large gap between the expectant and practical quality of service for XL-RIS aided system.

To overcome the constant modulus constraint and fill the gap in quality of service, we propose a block coordinate descent (BCD) based scheme with majorization-minimization (MM) algorithm for the multi-beam design in XL-RIS aided near-field wireless communications.[1] The proposed scheme handles this constraint from two aspects. Firstly, the multi-beam design is an intractable non-convex problem due to this constraint. We utilize the MM algorithm to decompose this problem as a series of tractable sub-problems to be iteratively solved. Secondly, the solution space for the multi-beam design is limited due to this constraint, we introduce the phases for beam gains as an extra optimizable variable to enrich the degree of freedom for optimization. Finally, the multiple beams can be designed by alternately optimizing the above two aspects with the BCD strategy. Simulation results show that the proposed multi-beam design can achieve a superior quality of service

[1]Simulation codes are provided to reproduce the results presented in this article: http://oa.ee.tsinghua.edu.cn/dailinglong/publications/publications.html.

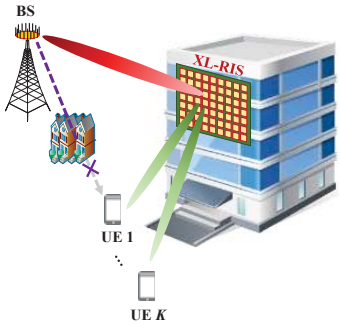

Fig. 1. The XL-RIS aided multi-UE wireless communication system.

50% higher than the existing schemes. Particularly, for far-field transmission, the proposed scheme also has a performance gain compared with the existing far-field schemes.

II. System Model

We firstly introduce the signal model, based on which the channel model for the XL-RIS aided near-field wireless communications is discussed.

A. Signal Model

We consider an XL-RIS aided wireless communication system, where a base station (BS) with M antennas is assisted by an XL-RIS with N elements to simultaneously serve K single-antenna UEs. Let $\mathcal{N}=\{1,2,\cdots,N\}$, and $\mathcal{K}=\{1,2,\cdots,K\}$ denote the index sets of XL-RIS elements, and UEs, respectively. The uniform linear array (ULA) of antennas is employed at the BS, and the uniform planar array (UPA) of elements is employed at the XL-RIS with N_1 horizontal rows and N_2 vertical columns ($N=N_1\times N_2$). We adopt the assumption that the direct BS-UE transmission link is blocked by the obstacles [6], as illustrated in Fig. 1. The frequency division multiplexing is adopted to serve multiple UEs. Taking the kth UE as an example, the received signal y_k for this UE can be expressed as

$$y_k=\mathbf{h}_{r,k}^T\mathbf{\Theta}\mathbf{G}\mathbf{x}+n_k, \tag{1}$$

where $\mathbf{x}\in\mathbb{C}^{M\times 1}$ is the precoded transmitted signal at the BS; $\mathbf{h}_{r,k}^T\in\mathbb{C}^{1\times N}$, and $\mathbf{G}\in\mathbb{C}^{N\times M}$ denote the channel from the XL-RIS to the kth UE, and the channel from the BS to the XL-RIS, respectively; $\mathbf{\Theta}\in\mathbb{C}^{N\times N}$ represents the beamforming matrix of the XL-RIS; $n_k\sim\mathcal{CN}\left(0,\sigma_n^2\right)$ denotes the additive white Gaussian noise received at the kth UE.

The XL-RIS can adjust the phase of an incident signal by designing $\mathbf{\Theta}$ as $\mathbf{\Theta}\triangleq\mathrm{diag}\left(\boldsymbol{\theta}\right)=\mathrm{diag}\left(\theta_1,\cdots,\theta_n,\cdots,\theta_N\right)$, where $\boldsymbol{\theta}$ represents the XL-RIS beamforming vector, and $\theta_n=e^{jp_n}$ $(p_n\in[0,2\pi],n\in\mathcal{N})$ represents the reflecting coefficient of the nth XL-RIS element. Then, the received signal model in (1) can be further represented as $y_k=\boldsymbol{\theta}^T\mathrm{diag}\left(\mathbf{h}_{r,k}^T\right)\mathbf{G}\mathbf{x}+n_k$, where the reflecting channel for the kth UE can be denoted as $\mathbf{H}=\mathrm{diag}\left(\mathbf{h}_{r,k}^T\right)\mathbf{G}$.

B. Channel Model

Before giving the near-field channel model, we briefly introduce the existing far-field Saleh-Valenzuela channel model [2]. The BS-RIS channel $\mathbf{G}^{\mathrm{FF}}$ can be denoted as $\mathbf{G}^{\mathrm{FF}}=\sum_{i=1}^{L_1}\alpha_i\mathbf{b}\left(\phi_{\mathrm{in},i},\varphi_{\mathrm{in},i}\right)\mathbf{a}^H\left(\gamma_i\right)$, where L_1 is the number of dominant paths, α_i is the complex gain of the ith path, $\phi_{\mathrm{in},i}$, and $\varphi_{\mathrm{in},i}$ represent the azimuth and elevation angles-of-arrival (AoAs) at the XL-RIS for the ith path, γ_i denotes the angle-of-departure (AoD) for the ith path at the BS. $\mathbf{a}\left(\gamma\right)$ and $\mathbf{b}\left(\phi,\varphi\right)$ are the far-field array steering vectors for the BS and the XL-RIS, respectively. Under the far-field planar wavefront assumption [4], these vectors can be denoted as $\mathbf{a}\left(\gamma\right)=\frac{1}{\sqrt{M}}\left[e^{j2\pi m\gamma}\right]_{m\in\mathcal{I}(M)}^T$ and $\mathbf{b}\left(\phi,\varphi\right)=\frac{1}{\sqrt{N}}\left[e^{j2\pi n_1\phi}\right]_{n_1\in\mathcal{I}(N_1)}^T\otimes\left[e^{j2\pi n_2\varphi}\right]_{n_2\in\mathcal{I}(N_2)}^T$, where the integer sequence $\mathcal{I}\left(n\right)$ can be expressed as $\mathcal{I}\left(n\right)=\{0,1,\cdots,n-1\}$.

Similarly, the RIS-UE channel in the far-field can be denoted as $\mathbf{h}_{r,k}^{\mathrm{FF}}=\sum_{l=1}^{L_2}\beta_{k,l}\mathbf{b}\left(\phi_{\mathrm{re},k,l},\varphi_{\mathrm{re},k,l}\right)$, where L_2 is the number of dominant paths, $\beta_{k,l}$ is the complex gain of the l-th path, $\phi_{\mathrm{re},k,l}$ and $\varphi_{\mathrm{re},k,l}$ are the azimuth and elevation AoDs at the XL-RIS for the lth path.

Note that the BS and XL-RIS are usually deployed in the high building, based on which there are few scatterers between the BS and XL-RIS. For high-frequency transmission, we consider that there is only the line-of-sight (LoS) path from the XL-RIS to the BS or UEs [6]. Meanwhile, since the deployment positions for the BS and XL-RIS are known and fixed, we assume for simplicity that the precoding at the BS has been designed [2]. Thus, we can focus on the XL-RIS beamforming design. Specifically, we can denote the effective BS beamforming as $\mathbf{v}=\mathbf{a}^H\left(\gamma\right)$, based on which the effective reflecting channel for the far-field can be rewritten as

$$\bar{\mathbf{h}}_{\mathrm{FF},k}=\bar{\alpha}_k\mathrm{diag}\left(\mathbf{b}^T\left(\phi_{\mathrm{re},k},\varphi_{\mathrm{re},k}\right)\right)\mathbf{b}\left(\phi_{\mathrm{in}},\varphi_{\mathrm{in}}\right), \tag{2}$$

where $\alpha_k=\bar{\alpha}\beta_k$ is the effective gain. The subscript i and l have been omitted for simplicity since $i=l=1$.

According to the electromagnetic propagation feature, the region of radiation field can be divided into two parts: the far-field region and the near-field region, with the boundary called the Rayleigh distance Z [4]. The definition for Z is $Z=2D^2/\lambda$, where D is the array aperture, and λ is the carrier wavelength. For an XL-RIS system, when the distance r_{RB} between the XL-RIS and BS, and the distance r_{RU} between the XL-RIS and UE satisfy $\frac{r_{\mathrm{RB}}r_{\mathrm{RU}}}{r_{\mathrm{RB}}+r_{\mathrm{RU}}}<Z=\frac{2D^2}{\lambda}$, the reflecting channel should be modeled as the near-field channel under the accurate *spherical wavefront assumption* [4]. Conversely, the reflecting channel can be modeled as the far-field channel under the approximate *planar wavefront assumption*.

The Rayleigh distance is proportional to the square of D. For the array with a fixed element spacing, with the increase of the array aperture from RIS to XL-RIS, the Rayleigh distance will increase quadratically. Hence, the region for near-field will be expanded, based on which the BS and UEs are more likely to strew in the near-field region as illustrated in Fig. 2. As long as any one of the BS or UE is located in the near-field region of XL-RIS, the reflecting channel should be modeled as

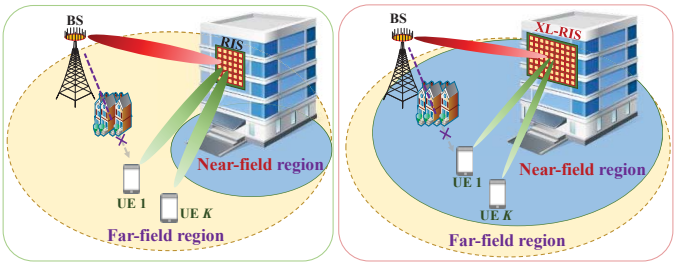

Fig. 2. The RIS aided far-field and the XL-RIS aided near-field wireless communications.

the near-field channel. Hence, for the XL-RIS aided wireless communications, the near-field propagation is more dominant under the spherical wavefront assumption [4].

Under the spherical wavefront assumption, for a same path, the AoAs (or AoDs) in different XL-RIS elements are no longer consistent. Hence, the channel phase in each element for XL-RIS is calculated independently, based on which the reflecting channel $\bar{\mathbf{h}}_{\mathrm{NF},k}$ can be modeled as

$$\bar{\mathbf{h}}_{\mathrm{NF},k} = \bar{\alpha}_k \mathrm{diag}\left(\mathbf{b}^T\left(\mathbf{r}_{\mathrm{re},k}\right)\right)\mathbf{b}\left(\mathbf{r}_{\mathrm{in}}\right), \tag{3}$$

where $\mathbf{r}_{\mathrm{re},k}$ is the space coordinates vector from the XL-RIS to the kth UE, and $\mathbf{r}_{\mathrm{in}}$ is the space coordinates vector from the BS to the XL-RIS. The steering vector in (3) can be expressed as [6]

$$\mathbf{b}\left(\mathbf{r}_{\mathrm{re},k}\right) = \Big[e^{-j2\pi D_k^{\mathrm{re}}(1,1)}, \cdots, e^{-j2\pi D_k^{\mathrm{re}}(1,N_2)}, \cdots, e^{-j2\pi D_k^{\mathrm{re}}(N_1,1)}, \cdots, e^{-j2\pi D_k^{\mathrm{re}}(N_1,N_2)}\Big]^T, \tag{4a}$$

$$\mathbf{b}\left(\mathbf{r}_{\mathrm{in}}\right) = \Big[e^{-j2\pi D^{\mathrm{in}}(1,1)}, \cdots, e^{-j2\pi D^{\mathrm{in}}(1,N_2)}, \cdots, e^{-j2\pi D^{\mathrm{in}}(N_1,1)}, \cdots, e^{-j2\pi D^{\mathrm{in}}(N_1,N_2)}\Big]^T, \tag{4b}$$

where $D_k^{\mathrm{re}}\left(n_1,n_2\right)$ and $D^{\mathrm{in}}\left(n_1,n_2\right)$ denote the distance from the (n_1,n_2)-th[2] element of the XL-RIS to the kth UE and the BS, respectively.

III. Proposed Near-Field Multi-Beam Design

In this section, we devise the near-field multi-beam design scheme for XL-RIS aided wireless communications. Note that this scheme is deployed based on the beam training, we also briefly introduce the existing beam training scheme at first.

A. The Beam Training Procedure

As mentioned in Section I, we can directly determine the XL-RIS beamforming vector by a codeword from a pre-designed codebook via beam training. This procedure is also the core operation of the single-beam design, which can be formulated as acquiring the desired XL-RIS beamforming $\boldsymbol{\theta}$ satisfying $\boldsymbol{\theta} = \arg\max_{\mathbf{c}_i \in \mathcal{C}} \left|\bar{\mathbf{h}}_{\mathrm{NF}}^T \mathbf{c}_i\right|$, where $\bar{\mathbf{h}}_{\mathrm{NF}}$ is the reflecting channel, and $\mathbf{c}_i$ is the codeword selected from the codebook $\mathcal{C}_{\mathrm{NF}}$ [6]. For the multi-UE case, this procedure can be performed sequentially, based on which we can acquire the XL-RIS beamforming for the kth UE as $\boldsymbol{\theta}_k$.

However, in the multi-UE case, a serious loss for the quality of service will be involved if we design the multiple beams by superposing these single beams $\{\boldsymbol{\theta}_k\}(k = 1, 2, \cdots, K)$ to simultaneously serve the multiple UEs. This is mainly because of the presence for constant modulus constraint in XL-RIS, i.e., the XL-RIS can only adjust the phase coefficient rather than the amplitude coefficient. Under this constraint, the solution space for multi-beam design cannot be projected onto linear space, thus the effective directions of the superposed beams will seriously deviate from the desired directions of UEs due to the nonlinear variation. To improve the quality of service, we explore the multi-beam design in the next subsection to handle the influence of the constant modulus constraint.

B. Proposed Multi-Beam Design Scheme

Before introducing the proposed scheme, we discuss the beam design in the far-field scenario as an example. Via beam training with DFT codebook [6] with S codewords[3], we can acquire the beam gain in all S discrete spatial angle grids by the power measurement. Hence, we can acquire the desired superposed beam gain $\mathbf{g} \in \mathbb{R}^{S\times 1}$ of all UEs in the S discrete spatial angles, based on which we can formulate the multi-beam optimization problem as

$$\begin{aligned} \mathcal{P}_{\mathrm{FF}}: \min_{\boldsymbol{\theta}} \quad & l_0 = \left\|\mathbf{g} - \mathbf{C}^H\boldsymbol{\theta}\right\|_2^2 \\ \text{s.t.} \quad & \mathrm{C}_1: |\theta_n| = 1, \forall n \in \mathcal{N}. \end{aligned} \tag{5}$$

This formulation is applicable for the far-field scenario. However, considering that the near-field channel is related to angles information as well as distance information, the near-field codebook grids S is much larger than that of the far-field DFT codebook, based on which it will bring higher computational complexity for the multi-beam design. Note that compared with the beam gains in each grids for the whole space, we care more about the beam gains pointing to the limited UEs' positions. Hence, we propose the near-field *multi-beam* design, where only the practical gain of K beams pointing to the desired K UEs as the desired gain $\bar{\mathbf{g}} \in \mathbb{R}^{K\times 1}$ are considered. Specifically, the multi-beam optimization problem can be expressed as

$$\begin{aligned} \mathcal{P}_{\mathrm{NF}}: \min_{\boldsymbol{\theta}} \quad & l_1 = \left\|\bar{\mathbf{g}} - \boldsymbol{\Xi}^H\boldsymbol{\theta}\right\|_2^2 \\ \text{s.t.} \quad & \mathrm{C}_1: |\theta_n| = 1, \forall n \in \mathcal{N}, \end{aligned} \tag{6}$$

where the kth column of the near-field steering matrix $\boldsymbol{\Xi} \in \mathbb{C}^{N\times K}$ is the codeword $\boldsymbol{\theta}_k$ for the kth UE acquired by beam training from the near-field codeword $\mathcal{C}_{\mathrm{NF}}$ [6].

Although the objective functions in $\mathcal{P}_{\mathrm{NF}}$ and $\mathcal{P}_{\mathrm{FF}}$ are similar, the optimization for $\mathcal{P}_{\mathrm{NF}}$ is more difficult. Specifically, this objective function of $\mathcal{P}_{\mathrm{NF}}$ can be rewritten as

$$l_1 = \bar{\mathbf{g}}^H\bar{\mathbf{g}} + \boldsymbol{\theta}^H\boldsymbol{\Xi}\boldsymbol{\Xi}^H\boldsymbol{\theta} - 2\mathrm{Re}\{\bar{\mathbf{g}}^H\boldsymbol{\Xi}^H\boldsymbol{\theta}\}. \tag{7}$$

[2]It means that this is the element located in the n_1th line and n_2th column of XL-RIS.

[3]We can write a codebook $\mathcal{C}$ by a matrix form as $\mathbf{C} \in \mathbb{C}^{N\times S}$ in this paper, where S is the codebook size, and codeword $\mathbf{c}_i$ is the ith column of this matrix.

Consider that in the far-field case, the codewords are usually orthogonal, i.e., we have $\mathbf{C}\mathbf{C}^H = \mathbf{I}_{N\times N}$. In this case, the optimization problem $\mathcal{P}_{\mathrm{NF}}$ is easy to be solved. This is mainly because the objective function can be simplified as $l_0 = \mathrm{Re}\{\mathbf{g}^H\mathbf{C}^H\boldsymbol{\theta}\}$ thanks to the orthogonality. However, for the matrix with size $N \times K$ ($K < N$), the result for $\boldsymbol{\Xi}\boldsymbol{\Xi}^H$ is an owe rank, i.e., we have $\boldsymbol{\Xi}\boldsymbol{\Xi}^H \neq \mathbf{I}_N$. As a result, $\mathcal{P}_{\mathrm{NF}}$ is a non-convex quadratic programming problem, which is difficult to be solved.

We propose a block coordinate descent (BCD) based scheme with majorization-minimization (MM) algorithm to solve this problem. The basic idea of the proposed scheme can be summarized as two aspects.

Firstly, we adopt the MM algorithm to solve the problem $\tilde{\mathcal{P}}_{\mathrm{NF}}$ to acquire the optimization of $\boldsymbol{\theta}$. The basic idea of the MM algorithm can be expressed as follows. For a difficult non-convex problem, we tackle it by dividing it to a series of approximate sub-problems, which are more tractable [8]. To iteratively solve these sub-problems in sequence, we can approach the optimal solution of the original objective function. Each iterative optimization is corresponding to a sub-problem.

Specifically, for a optimization problem $\min_{\boldsymbol{x}} f(\boldsymbol{x})$ subjecting to $\boldsymbol{x} \in \mathcal{X}$, a serious proxy functions $\{q(\boldsymbol{x}|\boldsymbol{x}^t)\}(t = 1, 2, \cdots)$ will be constructed according to the MM algorithm. Each proxy function can be treated as the objective function of the sub-problem. $q(\boldsymbol{x}|\boldsymbol{x}^t)$ is objective function for the tth iteration, and we denote $\boldsymbol{x}^{t+1} = \arg\min_{\boldsymbol{x}} q(\boldsymbol{x}|\boldsymbol{x}^t)$. To solve the original problem, it is important to appropriately design the proxy functions $\{q(\boldsymbol{x}|\boldsymbol{x}^t)\}$. Taking the tth iteration as an example, $q(\boldsymbol{x}|\boldsymbol{x}^t)$ is fulfilled the following four features as

$$f(\boldsymbol{x}) \leq q\left(\boldsymbol{x} \mid \boldsymbol{x}^t\right), \forall \boldsymbol{x} \in \mathcal{X}, \tag{8a}$$
$$f\left(\boldsymbol{x}\right) = q\left(\boldsymbol{x} \mid \boldsymbol{x}^t\right) \leftrightarrow \boldsymbol{x} = \boldsymbol{x}^t, \tag{8b}$$
$$\nabla_{\boldsymbol{x}} f\left(\boldsymbol{x}\right)\big|_{\boldsymbol{x}=\boldsymbol{x}^t} = \nabla_{\boldsymbol{x}} q\left(\boldsymbol{x} \mid \boldsymbol{x}^t\right)\big|_{\boldsymbol{x}=\boldsymbol{x}^t}, \tag{8c}$$
$$q(\boldsymbol{x}^{t+1}|\boldsymbol{x}^t) = \min q(\boldsymbol{x}|\boldsymbol{x}^t) \leftrightarrow \boldsymbol{x} = \boldsymbol{x}^{t+1}. \tag{8d}$$

The first feature in (8a) ensures that each proxy function is the upper bound of the original objective function. The second and third features in (8b) and (8c) mean that in the unique intersection point, the first-order gradient should be equal between the original objective function and the proxy function. On this basis, it can be guaranteed with the last feature in (8d) that this upper bound is strictly decreasing from the tth iteration to the $(t+1)$th iteration, based on which we have $f(\boldsymbol{x}^{t+1}) \leq q\left(\boldsymbol{x}^{t+1} \mid \boldsymbol{x}^t\right) \leq q\left(\boldsymbol{x}^t \mid \boldsymbol{x}^t\right) \leq f(\boldsymbol{x}^t)$. By solving the sub-problems $\mathcal{P}_t : \min_{\boldsymbol{x}} q\left(\boldsymbol{x} \mid \boldsymbol{x}^t\right)$ s.t. $\mathrm{C}_1 : \quad \boldsymbol{x} \in \mathcal{X}$, corresponding to the sequences of $\{q(\boldsymbol{x}|\boldsymbol{x}^t)\}, (t = 1, 2, \cdots)$, the optimal values of $\mathcal{P}_t$ is monotonically decreasing about t and finally converges to the optimal value of original problem.

Hence, for the difficult original objective function in (6), the core task is to design a suitable proxy function $\{q(\boldsymbol{x}|\boldsymbol{x}^t)\}$, which is much easier to be tackled than (6) and meeting the above four features. For convenience to discuss this issue, the optimization problem can be re-formulated according to (7) as

$$\mathcal{P}_{\mathrm{NF}} : \min_{\boldsymbol{\theta}, \boldsymbol{\varpi}} \quad l = \boldsymbol{\theta}^H\boldsymbol{\Xi}\boldsymbol{\Xi}^H\boldsymbol{\theta} - 2\mathrm{Re}\{\bar{\mathbf{g}}^H\boldsymbol{\Xi}^H\boldsymbol{\theta}\} \tag{9a}$$
$$\text{s.t.} \quad \mathrm{C}_1 : |\theta_n| = 1, \forall n \in \mathcal{N}. \tag{9b}$$

Then, we give the **Lemma 1** as the effective strategy for designing $q(\boldsymbol{\theta}|\boldsymbol{\theta}^t)$ to optimize $\boldsymbol{\theta}$ in the tth iteration.

Lemma 1: *The proxy function $q(\boldsymbol{\theta}|\boldsymbol{\theta}^t)$ fulfilling the above four features can be defined as*

$$\begin{aligned} &l = \boldsymbol{\theta}^H\boldsymbol{\Xi}\boldsymbol{\Xi}^H\boldsymbol{\theta} - 2\mathrm{Re}\{\bar{\mathbf{g}}^H\boldsymbol{\Xi}^H\boldsymbol{\theta}\} \leq \\ &q(\boldsymbol{\theta}|\boldsymbol{\theta}^t) \triangleq \boldsymbol{\theta}^H\mathbf{M}\boldsymbol{\theta} + 2\mathrm{Re}\{\boldsymbol{\theta}^H\left(\boldsymbol{\Xi}\boldsymbol{\Xi}^H - \mathbf{M}\right)\boldsymbol{\theta}^t\} + \\ &\boldsymbol{\theta}^{tH}(\mathbf{M} - \boldsymbol{\Xi}\boldsymbol{\Xi}^H)\boldsymbol{\theta}^t - 2\mathrm{Re}\{\bar{\mathbf{g}}^H\boldsymbol{\Xi}^H\boldsymbol{\theta}\}, \end{aligned} \tag{10}$$

for any given $\boldsymbol{\theta}^t$ and any available $\boldsymbol{\theta}$, where $\mathbf{M} \triangleq \lambda_{\max}\mathbf{I}_{N\times N}$ with $\lambda_{\max}$ denoting the maximum eigenvalue of $\boldsymbol{\Xi}\boldsymbol{\Xi}^H$.

Proof: See Appendix A. ■

With the guidance from **Lemma 1**, the XL-RIS beamforming $\boldsymbol{\theta}$ can be optimized by a iterative procedure to solve the minimization with a serious of $\{q(\boldsymbol{\theta}|\boldsymbol{\theta}^t)\}, (t = 1, 2, \cdots)$. Specifically, for tth iteration, the optimization can be expressed as $\boldsymbol{\theta}^{t+1} = \exp(j\angle(\boldsymbol{\Xi}\bar{\mathbf{g}} - \boldsymbol{\Xi}\boldsymbol{\Xi}^H\boldsymbol{\theta}^t + \lambda_{\max}\boldsymbol{\theta}^t))$.

Secondly, the constant modulus constraint results in the incomplete solution space of beam optimization. Hence, we introduce the phases for multi-beam gains as an extra optimizable variable to enrich the degree of freedom of optimization objective. Specifically, we introduce the phase factor $\boldsymbol{\varpi} = [e^{j\zeta_1}, e^{j\zeta_2}, \cdots, e^{j\zeta_K}]$ of beam gain as the optimizable variable. This will not change the optimization goal, since the desired beam gain is only corresponding to the amplitude, i.e., $\bar{\mathbf{g}}$. By denoting $\tilde{\mathbf{g}} = \bar{\mathbf{g}} \odot \boldsymbol{\varpi}$ with $\odot$ as Hadamard product operator, (9) can be expressed as

$$\tilde{\mathcal{P}}_{\mathrm{NF}} : \min_{\boldsymbol{\theta}, \boldsymbol{\varpi}} \quad l = \boldsymbol{\theta}^H\boldsymbol{\Xi}\boldsymbol{\Xi}^H\boldsymbol{\theta} - 2\mathrm{Re}\{\tilde{\mathbf{g}}^H\boldsymbol{\Xi}^H\boldsymbol{\theta}\} \tag{11a}$$
$$\text{s.t.} \quad \mathrm{C}_1 : |\theta_n| = 1, \forall n \in \mathcal{N}, \tag{11b}$$
$$\mathrm{C}_2 : \varpi_k = e^{j\zeta_k}, \forall k \in \mathcal{K}, \zeta_k \in [0, 2\pi]. \tag{11c}$$

For a given $\boldsymbol{\theta}^t$, the phase factor $\boldsymbol{\varpi}$ can be optimized as $\boldsymbol{\varpi} = \exp(j\angle(\boldsymbol{\Xi}^H\boldsymbol{\theta}^t))$.

According to the above two steps, the variable $\boldsymbol{\theta}$ and $\boldsymbol{\varpi}$ can be alternately optimized with the BCD strategy. For clarity, we summarize the whole process of this proposed BCD-based multi-beam design in **Algorithm 1**, based on which we can acquire the solution for XL-RIS beamforming as $\boldsymbol{\theta}^{\mathrm{opt}}$.

The calculation complexity for the closed-form solution for $\boldsymbol{\theta}$ and $\boldsymbol{\varpi}$ can be expressed as $\mathcal{O}(LKN)$, with L as the iteration times. For calculating the eigenvalue of $\boldsymbol{\Xi}\boldsymbol{\Xi}^H \in \mathbb{C}^{N\times N}$, the complexity is $\mathcal{O}(N^3)$. To reduce this complexity, we give the Proposition 1 as a straightforward trick, based on which the complexity for calculating the eigenvalue can be significantly reduced to $\mathcal{O}(K^3)$ rather than $\mathcal{O}(N^3)$, where we usually have $K \ll N$.

Proposition 1: *The calculation for $\lambda_{\max}$ is with the equivalent to acquire the maximum eigenvalue of the K-dimension square matrix $\mathbf{T} \in \mathbb{C}^{K\times K}$, if we have $\mathbf{T} = \boldsymbol{\Xi}^H\boldsymbol{\Xi}$.*

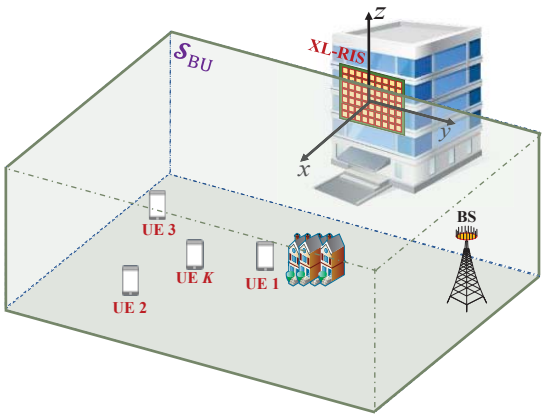

Fig. 3. An illustration of the simulation scenario.

Proof: By utilizing the singular value decomposition (SVD), we can expressed $\boldsymbol{\Xi} \in \mathbb{C}^{N\times K}$ as $\boldsymbol{\Xi} = \boldsymbol{U}\boldsymbol{\Sigma}\boldsymbol{V}^H$. Note that we have $\boldsymbol{\Xi}\boldsymbol{\Xi}^H = \boldsymbol{U}\boldsymbol{\Sigma}\boldsymbol{\Sigma}^H\boldsymbol{U}^H$ and $\mathbf{T} = \boldsymbol{V}\boldsymbol{\Sigma}^H\boldsymbol{\Sigma}\boldsymbol{V}^H$. According to the definition for eigenvalue, $\lambda_{\max}$ can be calculated from $\mathbf{T}$ with complexity $\mathcal{O}(K^3)$. ■

With Proposition 1, the complexity for the proposed scheme can be expressed as $\mathcal{O}(LKN) + \mathcal{O}(K^3)$.

Algorithm 1 BCD-Based Multi-Beam Design

Input: Desired beam gain $\bar{\mathbf{g}}$, maximum eigenvalue $\lambda_{\max}$, desirable accuracy ϵ, allowable threshold μ, maximum iteration $t_{\max}$, steering matrix $\boldsymbol{\Xi}$.

Output: Optimized reflecting vector $\boldsymbol{\theta}^{\text{opt}}$ for multi-beam design.

Init. initialized phase factor $\boldsymbol{\varpi}^{(0)}$, initialized reflecting vector $\boldsymbol{\theta}^{(0)}$, $i = 0$.
while $\left\|\tilde{\mathbf{g}}^{(i)} - \boldsymbol{\Xi}^H\boldsymbol{\theta}^{(i)}\right\|_2^2 \geq \epsilon$ **do**
  % 1) *Optimization for phase factor* $\boldsymbol{\varpi}^{(i+1)}$.
  $\boldsymbol{\varpi}^{(i+1)} = \exp(j\angle(\boldsymbol{\Xi}^H\boldsymbol{\theta}^{(i)}))$.
  $\tilde{\mathbf{g}}^{(i+1)} = \bar{\mathbf{g}} \odot \boldsymbol{\varpi}^{(i+1)}$.
  % 2) *Optimization for reflecting vector* $\boldsymbol{\theta}^{(i+1)}$.
  $\boldsymbol{\theta}^t|_{t=1} = \boldsymbol{\theta}^{(i)}$.
  for $t = 1$ **to** $t = t_{\max}$ **do**
    $\boldsymbol{\theta}^{t+1} = \exp(j\angle(\boldsymbol{\Xi}\tilde{\mathbf{g}}^{(i+1)} - \boldsymbol{\Xi}\boldsymbol{\Xi}^H\boldsymbol{\theta}^t + \lambda_{\max}\boldsymbol{\theta}^t))$.
    if $|\boldsymbol{\theta}^{t+1} - \boldsymbol{\theta}^t| < \mu$ **then**
      $\boldsymbol{\theta}^{(i+1)} = \boldsymbol{\theta}^{t+1}$.
      Break.
    else if $t = t_{\max}$ **then**
      $\boldsymbol{\theta}^{(i+1)} = \boldsymbol{\theta}^{t_{\max}+1}$.
      Break.
    else
      $t = t + 1$.
    end if
  end for
  $i = i + 1$.
end while
$\boldsymbol{\theta}^{\text{opt}} = \boldsymbol{\theta}^{(i)}$.

IV. Simulation Results

In this section, we provide the simulation results of the proposed multi-beam design in the XL-RIS aided near-field wireless communication system. Besides, the performance is also discussed in the far-field scenario.

TABLE I
Simulation Parameters Setup for the Near-field Scenario

Parameters	Value
Numbers of XL-RIS elements	$N_1 = 64$, $N_2 = 8$
Carrier frequency	$f = 10$ GHz
Element spacing for XL-RIS	$d_R = \lambda/2$
Number of UEs	$K \in [2, 20]$
Width of XL-RIS	$L_y = 0.12$ m
Height of XL-RIS	$L_z = 0.96$ m
Region for BS & UEs distribution	$\mathcal{R}_x = [200d_R, 1200d_R]$
Region for BS & UEs distribution	$\mathcal{R}_y = [-2500d_R, 2500d_R]$
Region for BS & UEs distribution	$\mathcal{R}_z = [-1000d_R, 0]$
Distance between UE & XL-RIS	$r \in [3, 44]$ m
Rayleigh distance	$Z = 62.4$ m

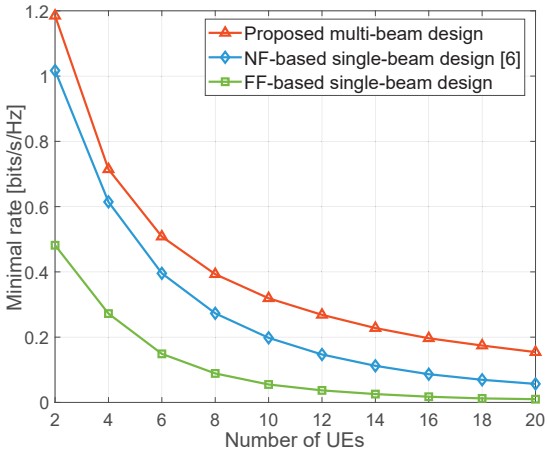

Fig. 4. Minimal rate performance comparison against the number of UEs.

A. Simulation Setup

1) Simulation scenario: We consider a three-dimensional scenario as shown in Fig. 3, where the XL-RIS is deployed on the yOz-plane with its center located at the origin of coordinate. The region for the XL-RIS can be expressed as $\mathcal{S}_{\text{R}} := \left\{(s_x, s_y, s_z) \middle| |s_x| = 0, |s_y| \leq \frac{L_y}{2}, |s_z| \leq \frac{L_z}{2}\right\}$, where L_y and L_z are the width and height of XL-RIS, i.e., we have $L_y = N_1\lambda/2$ and $L_z = N_2\lambda/2$. We assume that the BS and UEs are randomly distributed in the green color region in Fig. 3. This region can be expressed as $\mathcal{S}_{\text{BU}} := \left\{(s_x, s_y, s_z) \middle| s_x \in \mathcal{R}_x, s_y \in \mathcal{R}_y, s_z \in \mathcal{R}_z, \right\}$, where $\mathcal{R}_x = [R_{x,\min}, R_{x,\max}]$, $\mathcal{R}_y = [R_{y,\min}, R_{y,\max}]$, and $\mathcal{R}_z = [R_{z,\min}, R_{z,\max}]$, respectively.

2) Simulation parameters: The simulation parameters for the near-field scenario are determined following Table I. Note that the Rayleigh distance (62.4 m) is larger than 44 m, i.e., the maximum distance between XL-RIS and the UE (or BS). Hence, $\mathcal{S}_{\text{BU}}$ is located in the near-field region of XL-RIS.

3) Simulation baselines: We consider the existing near-field codebook based (NF-based) single-beam design [6] and the far-field (DFT) codebook based (FF-based) single-beam design as baselines. To serve multiple UEs, these single-beam design schemes superpose the beam design codewords for all UEs as the effective beamforming vector.

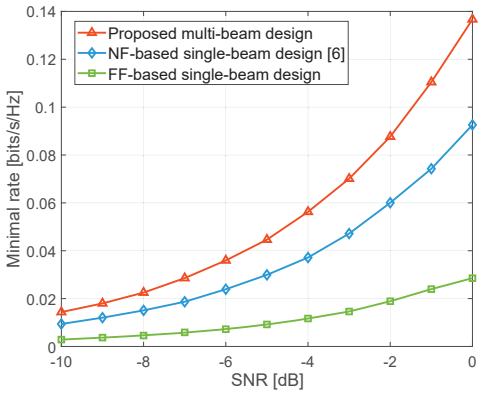

Fig. 5. Minimal rate performance comparison against the SNR.

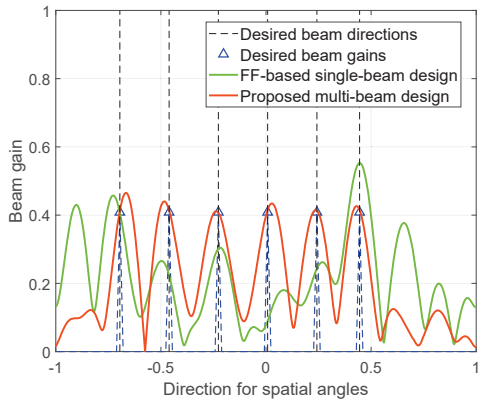

Fig. 6. The beam gains for multi-beam design.

B. Discussion for Simulation Results

To evaluate the quality of service, we choose the minimal rate as the performance indicator, which refers to the minimum achievable rates of all UEs.

Fig. 4 illustrates the minimal rate against the number of UEs. The received signal-to-noise ratio (SNR) is set as 5 dB. We can find that the minimal rate of proposed scheme is superior to the baselines. With $K = 10$, the minimal rate of the proposed scheme is 80% higher than the NF-based single-beam scheme.

Fig. 5 compares minimal rate performance against SNR. The number of UEs K is set as 8. Fig. 5 shows that the minimal rate for the proposed multi-beam design is better than the existing schemes in different SNRs. For example, with $\mathrm{SNR} = 0$ dB, the minimal rate for the proposed scheme is 50% higher than the NF-based single-beam scheme.

We also discuss our proposed scheme in the far-field scenario compared with the single beam design utilizing DFT codebook. We focus on the discussion for beam gain.

Fig. 6 considers a equipower multi-beam design scenario to generate beams pointing to six desired directions. Assuming the beam gain to generate one beam is 1, then the beam gain for multiple beams can be calculated as $\eta = \sqrt{1/6} \approx 0.4$ (i.e., $20\log_{10}\sqrt{1/6} \approx -8$ dB). Fig. 6 shows that the proposed scheme can provide multi-beams accurately pointing to the desired directions with desired beam gain.

V. Conclusions

We have investigated the multi-beam design problem in XL-RIS aided near-field wireless communications. Most of the existing works for near-field XL-RIS systems focused on the single-beam design, which will involve a serious loss for the quality of service in the multi-UE case due to the constant modulus constraint. To overcome this constraint, a BCD-based scheme with the MM algorithm has been proposed for the multi-beam design to serve multiple UEs. Simulation results have shown that the proposed scheme could achieve a superior quality of service 50% higher than the existing single-beam design schemes. Particularly, the proposed scheme also has a performance gain in the far-field scenario.

Appendix A
Proof Of Lemma 1

Limited by the pages constraints, we briefly give the core procedure. To calculate the second-order Taylor expansion for $\boldsymbol{\theta}^H \boldsymbol{\Xi}\boldsymbol{\Xi}^H \boldsymbol{\theta}$ at $\boldsymbol{\theta}^t$, we have

$$\begin{aligned}\boldsymbol{\theta}^H \boldsymbol{\Xi}\boldsymbol{\Xi}^H \boldsymbol{\theta} =& {\boldsymbol{\theta}^t}^H \boldsymbol{\Xi}\boldsymbol{\Xi}^H \boldsymbol{\theta}^t + 2\,\mathrm{Re}\left(\left(\boldsymbol{\theta}-\boldsymbol{\theta}^t\right)^H \boldsymbol{\Xi}\boldsymbol{\Xi}^H \boldsymbol{\theta}^t\right) \\ &+ \left(\boldsymbol{\theta}-\boldsymbol{\theta}^t\right)^H \boldsymbol{\Xi}\boldsymbol{\Xi}^H \left(\boldsymbol{\theta}-\boldsymbol{\theta}^t\right).\end{aligned} \tag{12}$$

Since $\mathbf{M} - \boldsymbol{\Xi}\boldsymbol{\Xi}^H \succeq \mathbf{O}$, we can relax the third item of Taylor expansion as $\left(\boldsymbol{\theta}-\boldsymbol{\theta}^t\right)^H \mathbf{M}\left(\boldsymbol{\theta}-\boldsymbol{\theta}^t\right)$, based on which the upper bound for l can be calculated as $q(\boldsymbol{\theta}|\boldsymbol{\theta}^t)$, which completes the proof of **Lemma 1**.

Acknowledgment

This work was supported in part by the National Key Research and Development Program of China (Grant No. 2020YFB1805005), in part by the National Natural Science Foundation of China (Grant No. 62031019), and in part by the European Commission through the H2020-MSCA-ITN META WIRELESS Research Project under Grant 956256.

References

[1] S. Ma, W. Shen, J. An, and L. Hanzo, "Wideband channel estimation for IRS-aided systems in the face of beam squint," *IEEE Trans. Wireless Commun.*, vol. 20, no. 10, pp. 6240–6253, Oct. 2021.

[2] S. Liu, Z. Gao, J. Zhang, M. D. Renzo, and M.-S. Alouini, "Deep denoising neural network assisted compressive channel estimation for mmWave intelligent reflecting surfaces," *IEEE Trans. Veh. Technol.*, vol. 69, no. 8, pp. 9223–9228, Aug. 2020.

[3] H. Sun, S. Zhang, J. Ma, and O. A. Dobre, "Path loss of RIS-aided spatial modulation with on/off pattern," *IEEE Commun. Lett.*, vol. 26, no. 4, pp. 937–941, Apr. 2022.

[4] M. Cui, Z. Wu, Y. Lu, X. Wei, and L. Dai, "Near-field communications for 6G: Fundamentals, challenges, potentials, and future directions," *arXiv preprint arXiv:2203.16318*, Mar. 2022.

[5] C. Feng, W. Shen, J. An, and L. Hanzo, "Joint hybrid and passive RIS-assisted beamforming for mmWave MIMO systems relying on dynamically configured subarrays," *IEEE Internet Things J.*, pp. 1–1, Jan. 2022.

[6] X. Wei, L. Dai, Y. Zhao, G. Yu, X. Duan, and X. Wang, "Codebook design and beam training for extremely large-scale RIS: Far-field or near-field?" *China Commun.*, vol. 19, no. 6, pp. 193–204, Jun. 2022.

[7] G. Alexandropoulos, V. Jamali, R. Schober, and V. Poor, "Near-field hierarchical beam management for RIS-enabled millimeter wave multi-antenna systems," *arXiv preprint arXiv:2203.15557*, Mar. 2022.

[8] Y. Sun, P. Babu, and D. P. Palomar, "Majorization-minimization algorithms in signal processing, communications, and machine learning," *IEEE Trans. Signal Process.*, vol. 65, no. 3, pp. 794–816, Feb. 2017.